Ultrafast, broadband and tunable terahertz reflector and neutral density filter based on high resistivity silicon

J. Degert, M. Tondusson, V. Freysz, E. Abraham, S. Kumar, Eric Freysz

Ultrafast, broadband and tunable terahertz reflector and neutral density filter based on high resistivity silicon

J. DEGERT,[1] M. TONDUSSON,[1] V. FREYSZ,[1] E. ABRAHAM,[1] S. KUMAR,[2] AND E. FREYSZ[1,*]

[1] *Univ. Bordeaux,CNRS, LOMA UMR 5798,Talence 33400, France*
[2] *Femtosecond Spectroscopy and Nonlinear Photonics Laboratory, Department of Physics, Indian Institute of Technology Delhi, New Delhi 110016, India*
[*] *eric.freysz@u-bordeaux.fr*

Abstract: We report THz transmission and reflection properties of an ultrafast optically excited highly resistive silicon wafer. Amplified Ti:Sapphire femtosecond laser pulses at 800 nm were used to create fluence-dependent carrier density on the front surface of the wafer which modifies the dielectric properties at the THz frequencies. Time-resolved experiments in the optical pump-THz probe configuration were conducted in which THz pulses reflected off from the surface at 0° and 45° angles of incidence make it possible to measure the pump-fluence dependent ultrafast evolution of the reflection and transmission coefficients in 0.5-6 THz range. An analytical model, where both the Drude contributions from the photoexcited electrons and holes account for the change of the dielectric constant of the photoexcited silicon, has been used to evaluate the THz reflection and transmission coefficients at steady state. Thus obtained results match well with the experimental results and demonstrate an all-optical means to convert a silicon wafer into an ultrafast, tunable and broadband neutral density filter or reflector in the THz frequency range.

1. Introduction

Ultrashort broadband as well as tunable continuous wave terahertz (THz) radiation is being used for many applications through new ideas and devices in different branches of science, engineering and medicine. From that standpoint, new materials and their use in innovative ways are always on top of the interest for dedicated applications in THz frequency range. Highly resistive silicon (HRSi) continues to have a special place for specific applications in electronics and optoelectronics. This material is readily available, almost transparent and dispersion free in the THz spectral range. However, in this semiconducting material the free carriers, which strongly interact with THz waves, have been shown to efficiently impact the absorption and dispersion properties [1–3]. The generation of free carriers following excitation of the HRSi by ultrashort laser pulses, modulates its dielectric constant. In fact, photo-excited HRSi has been studied for various applications such as anti-reflection coatings [4], highly reflective materials [4, 5], and reflection switches [5, 6], to name a few. The change in the THz properties of HRSi upon pulsed laser excitation has been reported by different authors using optical-pump THz-probe experiments [3–5, 7]. To analyze the change in properties of HRSi, numerical simulations using Drude model have been reported [3]. For low pump fluence, where the photo-excited layer can be considered to be very thin, simple analysis can be performed [4]. For higher pump fluence, analytical expressions for the reflectivity and transmissivity of a semiconductor, in which an exponentially distributed carrier concentration is photo-induced, has been derived [8]. The latter expression, which accounts for the change of silicon properties in the visible spectral range, can be straightforwardly extended to the THz frequencies.

Hereafter, we report on the evolution of the transmission and reflection coefficients of an ultrashort THz pulse by an HRSi wafer upon its excitation by amplified Ti:Sapphire femtosecond laser pulses. These experiments performed at 0° and 45° angle of incidence make it possible to measure the evolution of the reflection and transmission coefficients on photoexcited HRSi on the 0.5-6 THz frequency range. The latter data are compared with our computations performed using analytical expressions. Experiments and computations are found to be in agreement when realistic experimental conditions about the spatial distributions of the pump pulse and different spectral components of the THz pulse are considered. This ensemble of results underlines that upon excitation HRSi is an interesting means to provide ultrafast, broadband and tunable density filters or reflectors in the THz frequency range.

2. Experimental setup

The setup we used to run the experiment is displayed in Fig. 1a. It has been detailed in our previous works [9, 10]. The THz pulses were generated focusing in air ~ 1 mJ of the fundamental and second harmonic of Ti:Sapphire laser pulses. At the focal point, a plasma is induced and generates a broadband and ultra-short THz pulse. The THz pulse is focused on a 1 mm thick float zone HRSi wafer supplied by Tydex. The THz pulse reflected or transmitted by the sample is collimated and then sampled in time performing an electro-optic detection using a 200 µm thick ⟨110⟩ GaP crystal optically contacted on 3 mm thick ⟨100⟩ GaP crystal. The sample is excited by a pump pulse centered at 800 nm transmitted by a small hole drilled in the parabolic mirror used to focus the THz pulse on the sample. The time delay between the pump and THz pulses is adjusted with a delay line. On the sample the waist size of the pump beam is $w_{pump} = 700 \pm 20\,\mu m$. Hereafter, only p-polarized THz pulses transmitted at normal incidence or reflected at 45° angle of incidence are reported.

The electric field of the THz pulses we generated with our setup is displayed in black in Fig. 2a. Its Fourier spectrum, limited by the acceptance bandwidth of our GaP sampling crystal, spans in between 0.1 and 8 THz. At the sample position, the THz pulse is tightly focused by the parabolic mirror. Therefore the beam size of the different THz spectral components is likely to evolve. To confirm this, we used a knife edge technique. The knife edge was moved across the THz beam and the THz pulses transmitted at normal incidence were sampled in time. The evolution of the transmitted THz spectrum versus the knife edge position makes it possible to infer the beam size of the different THz spectral components. As shown in Fig. 1b, the waist size of the THz beam linearly decreases as the frequency increases. It is ~ 1.6 mm at 0.5 THz and

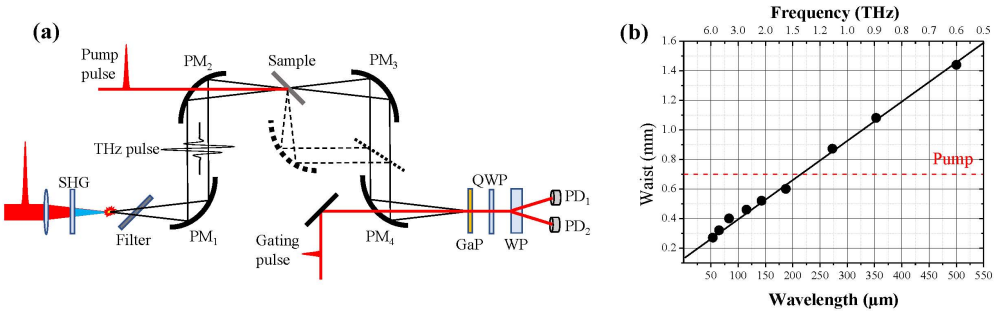

Fig. 1. Setup of the optical-pump THz-probe experiment. PM, parabolic off-axis mirror; QWP, quarter-wave plate; WP, Wollaston prism; PD: photodiode. b) Evolution of the waist size of the THz beam on the sample versus the wavelength or THz frequency. The black line is a linear fit of the waist size versus the THz frequencies. The dashed red line indicates the pump waist size seen by the different THz spectral components.

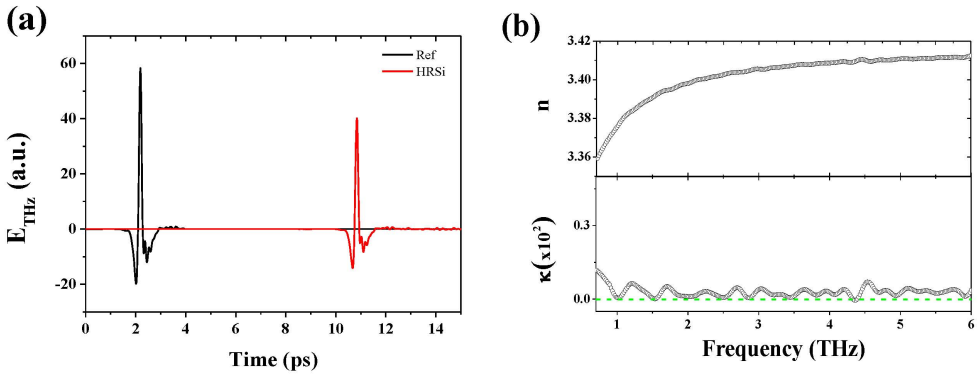

Fig. 2. a) In black the temporal evolution of the THz pulse generated in our setup. In red, temporal evolution of the THz pulse transmitted by the HRSi wafer. b) Evolution of the real part of the index of refraction n and extinction coefficient κ of the HRSi wafer in between 0.7 and 6 THz.

decreases to ~ 0.27 mm at 6 THz. Hence, the waist size of part of THz spectral components are higher than the pump waist size ($\sim 700\,\mu$m).

3. Experimental results.

We insert the HRSi wafer at the sample position and record the THz field transmitted at normal incidence (in red in Fig. 2a). The latter is delayed in time and its amplitude is reduced. Knowing the thickness of the sample, we infer both the real n and imaginary part κ of the index of refraction [11]. The results of these computations (Figs.2) are in good agreement with the literature [1]. The index n_0 of the HRSi is ~ 3.377 at 1 THz and increases to ~ 3.413 at 7 THz. The absorption coefficient $\alpha = 4\pi\kappa/\lambda_{THz}$ remains below 10 cm^{-1} in between 0.1 and 7 THz and it is less than 0.1% for a 1 mm thick HRSi.

Knowing the index of refraction of our HRSi sample in the THz spectral range, one can readily compute the reflection coefficient r and the transmission coefficient t at the air/HRSi interface. At normal incidence $r \sim 0.55$ and $t \sim 0.45$ whereas at 45° of incidence and for a p-polarized wave $r_p \sim 0.43$ and $t_p \sim 0.42$. It is worth mentioning the contribution of κ ($\kappa \ll n_0$) can be neglected and the dispersion of the index of refraction do not significantly impact the evolution of these reflection or transmission coefficients. Hereafter, we will consider $n_0 = \sqrt{\varepsilon_{HRSi}} \sim 3.41$.

Then we sampled the THz pulse at its maximum and recorded its amplitude variation upon excitation of the HRSi for various pump pulse energies and different pump pulse delays (Fig. 3a) at normal incidence. Upon excitation, the transmitted THz pulse decreases rapidly within ~ 1 ps, remains constant for ~ 900 ps and then decreases (not shown). For the pump - THz delay $\Delta T = 10$ ps, the evolution of the transmission coefficient of the HRSi wafer versus the pump pulse energy is displayed in Fig. 3b. The transmission of the photo-excited HRSi decreases rapidly as the pump pulse energy increases. Initially $\sim 70\%$, it drops below 10% when the pump pulse energy is $> 40\,\mu$J. We also recorded the temporal shape of the THz pulse at $\Delta T = 10$ ps (Fig. 4a). One can notice the maximum of the THz pulse is delayed in time as the energy of the pump pulse increases. This phenomenon, previously reported for photoexcited GaAs surfaces [12], indicates that Fig. 3b does not properly reflect the evolution of the actual maximum of the transmitted THz pulse, mainly owing to the modification of the THz pulse spectrum by the photo-generated carriers. The Fourier transform of the temporal shape of the pulse displayed in Fig. 4a makes it possible to compute the evolution of the spectral amplitude of the transmitted THz pulse (Fig. 4b).

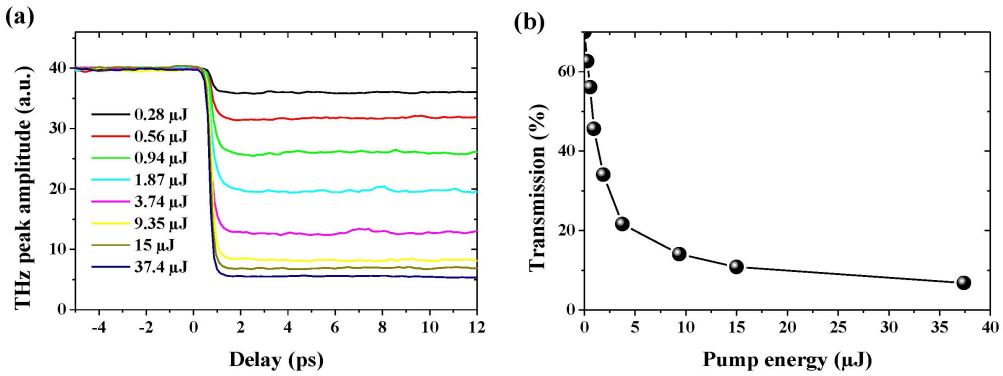

Fig. 3. a) Evolution at normal incidence of the maximum of the THz pulse for different pump energies and versus the pump pulse delay. b) Transmission coefficient at normal incidence of the silicon wafer for a 10 ps pump delay after the beginning of the decrease of the THz peak amplitude for the different pump pulse energies. Prior to its excitation, the transmission of the HRSi wafer is ~ 70%

As the pump pulse energy increases the amplitude of the transmitted THz spectral components steadily decreases. As displayed in Fig. 4c, at a given pump pulse energy the amplitude of the transmission coefficient remains almost constant over 1 to 6 THz spectral range. Figure 4d

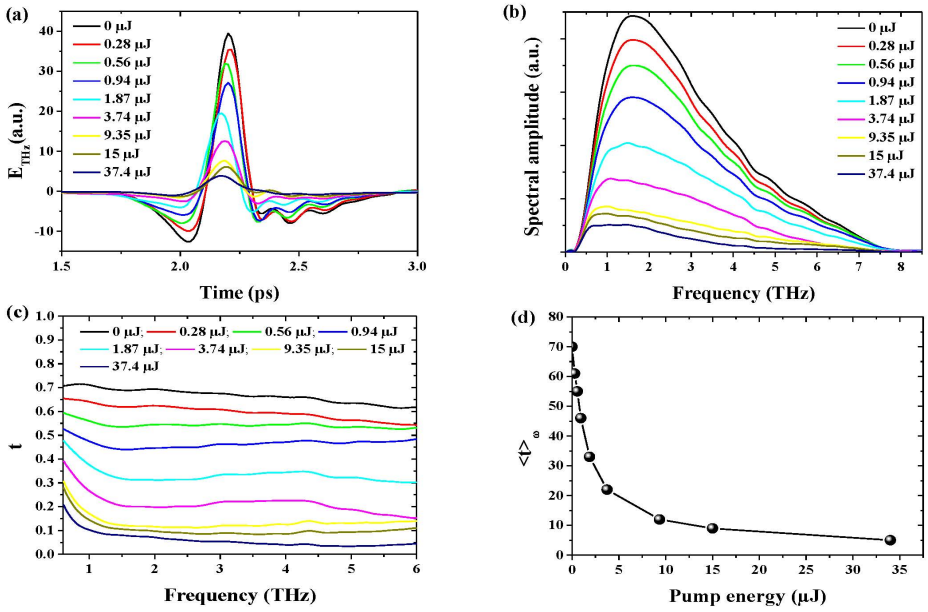

Fig. 4. a) Evolution of the THz pulse transmitted by the HRSi at $\Delta T = 10$ ps for various pump pulse energies. b) Spectral amplitude of the THz pulse transmitted by the HRSi at $\Delta T = 10$ ps for various pump pulse energies. c) Evolution of the transmission coefficient $t(\omega)$ of the different spectral components of the THz pulse versus the pump pulse energy at $\Delta T = 10$ ps. d) Evolution of the overall transmitted THz spectral amplitude $\langle t(\omega)\rangle_\omega$, versus the pump pulse energy at $\Delta T = 10$ ps.

reports the evolution of the area beneath the transmission coefficient. It indicates the THz pulse transmitted by the HRSi wafer is drastically reduced as the pump pulse energy increases. Initially $\sim 70\%$, it decreases below 12% when the pump pulse energy is larger than 10 µJ. This results shows that upon excitation HRSi wafer behaves as an ultrafast broadband neutral density filter with transmission ranging from 0.155 to 1.3 in the 1-6 THz frequency range.

We also recorded the amplitude of THz pulses reflected at 45° angle of incidence for collinear and p-polarized pump and THz pulses. For this measurement, a thin Teflon piece is inserted along the propagation axis of the THz pulse to filter out the reflected pump pulse. The evolution of the reflected THz pulse at its maximum versus the pump pulse energy and time delay is displayed in Fig. 5a. When the pump pulse energy is higher than 1 μJ, the amplitude of the THz signal increases within $\sim$ 1 ps, remains constant for $\sim$ 900 ps and then decreases (not shown). Knowing the reference and the THz signal reflected by the HRSi wafer prior to its excitation, we readily computed the evolution of the THz peak reflection coefficient versus the pump pulse energy (Fig. 5b). The latter, initially $\sim 43\%$, increases to about $\sim 80\%$ and seems to saturate for pump pulse energies higher than 100 µJ. We also sampled the THz pulse reflected by the HRSi wafer 10 ps after its excitation (Fig. 5c) at various pump pulse energies and computed the evolution of the reflection coefficient of the reflected THz pulse in the spectral range (Fig. 5d). For low pump pulse energy, the reflection coefficient is slightly below 0.43 between 3 and 6 THz, indicating the excited HRSi wafer is partly anti-reflective in this spectral range. This phenomenon was previously reported [4]. Here we demonstrate it only occurs in a given spectral range that strongly depends on the pump pulse intensity. This indicates that upon excitation HRSi wafer behaves as an ultrafast broadband and tunable reflector

4. Model for laser induced modulation of THz transmission and reflection in silicon wafer.

The impact of the laser pulse absorbed by silicon wafers on their optical properties in the THz frequency range has been proposed by different authors. The basic idea is that the photo-generated carriers produced by the pump pulse E_p modify the dielectric constant $\epsilon(\omega)$ of the material. In a damped Drude representation where both generated electrons and holes contribute, the permittivity of the excited silicon writes:

$$\epsilon(\omega) = \epsilon_{HRSi} - \frac{\omega_{p,e}^2}{\omega\left(\omega + i/\tau_{D,e}\right)} - \frac{\omega_{p,h}^2}{\omega\left(\omega + i/\tau_{D,h}\right)}, \tag{1}$$

where ϵ_{HRSi}, taken to be 11.68, is the permittivity of the unexcited HRSi sample in the THz frequency range. The electron and hole plasma frequency are $\omega_{p,(e,h)}^2 = N_{e,h}e^2/m_{e,h}^*\varepsilon_0$ where $N_{e,h}$ is the density of photo-generated electrons and holes, e is the elementary charge and ε_0 is the vacuum permittivity. For HRSi the effective mass of electrons and holes are taken to be $m_e^* = 0.2588\ m_e$ and $m_h^* = 0.2063\ m_e$, respectively, where m_e is the electron rest mass. $\tau_{D,e} = 0.199$ ps and $\tau_{D,h} = 0.056$ ps are the Drude's damping time for electrons and holes, respectively [6]. Assuming a quantum efficiency of 1, the spatial distribution of the density of electron-hole pairs generated by a pump laser with a spatially Gaussian radial fluence $F(r) = F_0\ \exp(-\frac{2r^2}{w_{pump}^2})$ writes $N_{e,h}(r) = (1-R)\alpha_p\lambda F(r)/(hc)$ where c, h, r, $R \sim 0.33$ and $\alpha_p \sim 8.3 \times 10^4 \mathrm{m}^{-1}$ are the speed of light in vacuum, the Planck's constant, the radial position, the absorption coefficient of HRSi at the pump wavelength $\lambda = 800$ nm, respectively. Since, experimentally, the transmission and reflection coefficient of HRSi remain almost unchanged in between 1 ps and 900 ps upon its photo-excitation, we will consider the photo-induced electron-hole density $N_{e,h}(r)$ remains constant during that lapse of time. Besides, we will also consider that, like for the pump pulse energy, $N_{e,h}(r)$ and $\epsilon(\omega, r)$ decay exponentially within the HRSi wafer and accordingly:

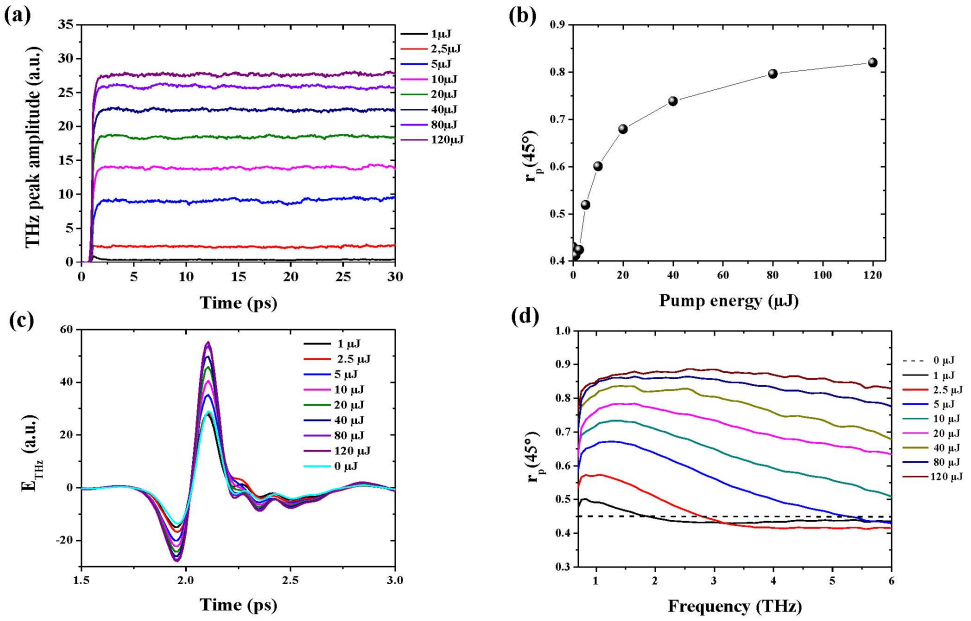

Fig. 5. a) Impact of the p-polarized pump pulse energy on the amplitude of a p-polarized THz pulse reflected at 45° by HRSi 10 ps after its photo-excitation. b) Impact of the p-polarized pump pulse energy on the reflection coefficient measured at the THz peak of a p-polarized THz pulse reflected at 45° by HRSi 10 ps after its photo-excitation. c) Temporal evolution of a p-polarized THz pulse reflected at 45° by the HRSi wafer 10 ps after its photo-excitation by p-polarized pump pulse. d) Evolution of reflection coefficient for the spectral component of a p-polarized THz pulse reflected at 45° by the HRSi wafer 10 ps after its photo-excitation by p-polarized pump pulse.

$$\epsilon(\omega, r, x) = \epsilon_{HRSi} - \gamma(\omega, r) e^{-\alpha_p x}, \tag{2}$$

where $\gamma(\omega, r) = \frac{\omega_{p,e}^2(r)}{\omega\left(\omega + i/\tau_{D,e}\right)} + \frac{\omega_{p,h}^2(r)}{\omega\left(\omega + i/\tau_{D,h}\right)}$.

Inserting the Eq. 2 in the wave equation and writing the boundary conditions for the tangential components of the electric and magnetic fields, one can compute the reflection, $r_{exc}(r, x)$, transmission, $t_{exc}(r, x)$, coefficients and the amplitude $E(\omega, r, x)$ of the THz field at the position x within the HRSi wafer [8]. At normal incidence, the latter writes:

$$E(\omega, r, x) = c_2(\omega, r) E_{in}(\omega, r) J_{-m}[z(\omega, r, x)],$$

where $E_{in}(\omega, r)$ is the incident THz field at the radial position r, J_m is a Bessel function of the first kind and mth order, $z(\omega, r, x) = i z_0(\omega, r) e^{-\alpha_p x/2}$, $z_0(\omega, r) = 2\omega\sqrt{\gamma(\omega, r)}/(\alpha_p c)$, $m = 2i\omega n_0/(\alpha_p c)$ and

$$c_2(\omega, r) = \frac{2}{(1 + n_0) J_{-m}[i z_0(\omega, r)] + \sqrt{\gamma(\omega, r)} J_{-m+1}[i z_0(\omega, r)]}. \tag{3}$$

where $n_0 \sim 3.377$ is the index of the unexcited HRSi. It is worth mentioning that, as indicated in the experimental part, the waist $w_{THz}^2(\omega)$ of the THz beam varies from one spectral component to another. Hence, the incident THz field writes $E_{in}(\omega, r) = E_{0,in}(\omega)\ \exp(-r^2/w_{THz}^2(\omega))$.

The transmission $t_{exc}(\omega, r)$ and reflection $r_{exc}(\omega, r)$ coefficients of the photo-excited air/HRSi interface write $t_{exc}(\omega, r) = c_2(\omega, r) J_{-m}[iz_0(\omega, r)]$ and

$$r_{exc}(\omega, r) = \frac{r_0 - \Delta_0(\omega, r)}{1 + \Delta_0(\omega, r)}, \tag{4}$$

where

$$\Delta_0(\omega, r) = \frac{J_{-m+1}[iz_0(\omega, r)]\sqrt{\gamma(\omega, r)}}{J_{-m}[iz_0(\omega, r)](1 + n_0)}, \tag{5}$$

and $r_0 = (1 - n_0)/(1 + n_0)$. Finally, the transmission coefficient $t_{tot}(\omega, r)$ of the HRSi wafer that thickness $L \gg \alpha_p^{-1}$ writes:

$$t_{tot}(\omega, r) = c_2(\omega, r) J_{-m}[z(\omega, r, L)] \frac{2n_0}{n_0 + 1}, \tag{6}$$

where the factor $2n_0/(n_0 + 1)$ accounts for the transmission by the back unexcited surface of the HRSi wafer.

For an angle of incidence θ_0 and a p-polarized THz wave, $\Delta_0(\omega, r)$ is replaced by $\Delta_1(\omega, r)$ in Eq. (4) and the reflection coefficient becomes:

$$r_p(\omega, r, \theta_0) = \frac{r_0 - \Delta_1(\omega, r)}{1 + \Delta_1(\omega, r)}, \tag{7}$$

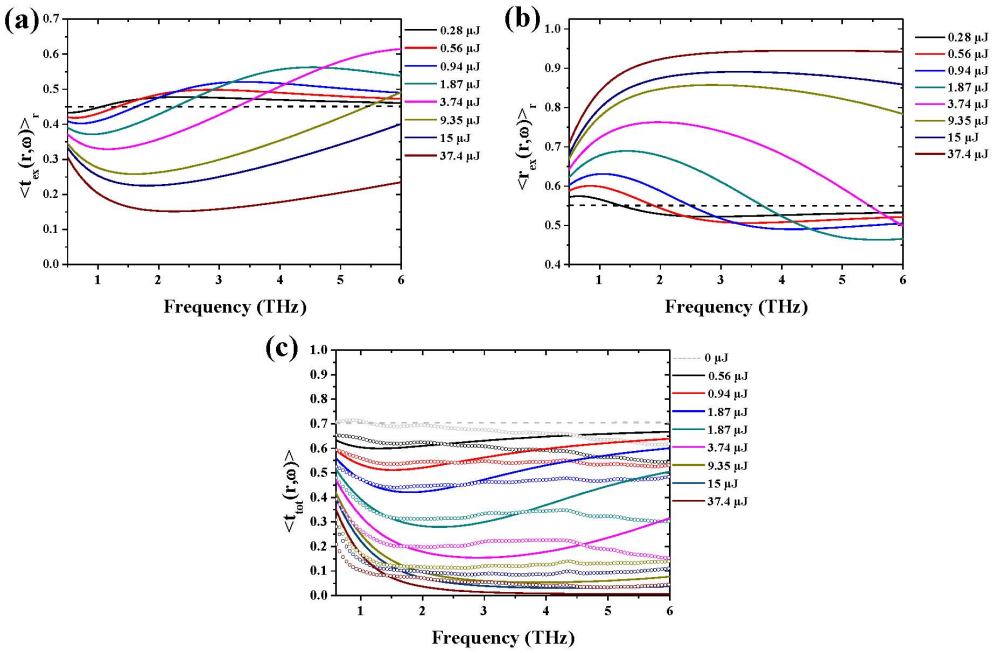

Fig. 6. a) Computed evolution of the transmission coefficient at normal incidence of the photo-excited air/HRSi interface versus the pump pulse energy. b) Computed evolution of the reflection coefficient at normal incidence of the photo-excited air/HRSi interface versus the pump pulse energy. c) Computed (solid line) and experimental (dots) evolution of the transmission coefficient at normal incidence of the photo-excited HRSi wafer versus the pump pulse energy.

where

$$\Delta_1(\omega, r) = \frac{J_{-m+1}[iz_0(\omega, r)]\sqrt{\gamma(\omega, r)}}{J_{-m}[iz_0(\omega, r)](\cos(\theta_1(r))/\cos(\theta_0) + n_0)}, \tag{8}$$

and $\theta_1(r)$ is the refraction angle within the HRSi. The latter is computed using expression for refraction at a metal surface [13].

In Fig. 6, we have plotted the evolution of $\langle t_{exc}(r,\omega)\rangle_r$, $\langle r_{exc}(r,\omega)\rangle_r$ and $\langle t_{tot}(r,\omega)\rangle_r$ in the 0.5 to 6 THz frequency range. The latter were computed integrating over the spatial profile of the pump and THz pulses according to their measured experimental beam sizes. It should be noted that for our thick HRSi wafer, $\langle t_{tot}(r,\omega)\rangle_r$ results from transmission by the excited air/HRSi interface, propagation in the HRSi wafer and transmission by the unexcited HRSI/air interface. The evolution of $\langle t_{tot}(r,\omega)\rangle_r$ versus the pump pulse energy agrees with our experimental data. However for high pump pulse energies, the experimental transmission coefficient remains always larger compared to the computed one. This behavior is likely due to the deviation from a Gaussian spatial distribution of the actual THz beam generated in emission from two-color laser-induced air plasma filaments [14–20]. When the pump pulse energy $0.3\,\mu J < E_p < 15\,\mu J$ and above 1 THz, the transmission $\langle t_{exc}(r,\omega)\rangle_r$ of the excited air/HRSi interface increases above its unexcited value (~ 0.45) underlying this photoexcited interface is partly antireflective. Consequently, $\langle r_{exc}(r,\omega)\rangle_r$ decreases below its unexcited value for frequencies above 1 THz (Fig. 6b). This phenomenon results from the shift of the plasma frequency induced by generation of carriers. When $E_p > 15\,\mu J$, the plasma frequency is shifted above 6 THz and $\langle r_{exc}(r,\omega)\rangle_r$ increases while $\langle t_{exc}(r,\omega)\rangle_r$ decreases. Surprisingly in Fig. 6c and whatever E_p, $\langle t_{tot}(r,\omega)\rangle_t$ is always smaller compared to the transmission of unexcited HRSi wafer ($t \sim 0.7$). In fact, even for low pump pulse energy, the increase in transmission of the excited air/HRSi interface is compensated by the large absorption of the very thin layer of photo-induced carriers. The absorption of the latter steadily increases with the pump pulse energy. This confirms that a photoexcited HRSi wafer behaves like a broadband density filter whose optical density can be efficiently switched and controlled on demand.

In Fig. 7, we display the evolution of the reflection coefficient $\langle r_p(r,\omega,\theta)\rangle_r$ of photoexcited air/HRSi interface for p-polarized THz wave for $\theta_0 = 45°$ and Brewster's angles ($\theta_{Brewster} \sim 74.7°$) of incidence versus the pump pulse energy. The p-polarized pump pulse is collinear with

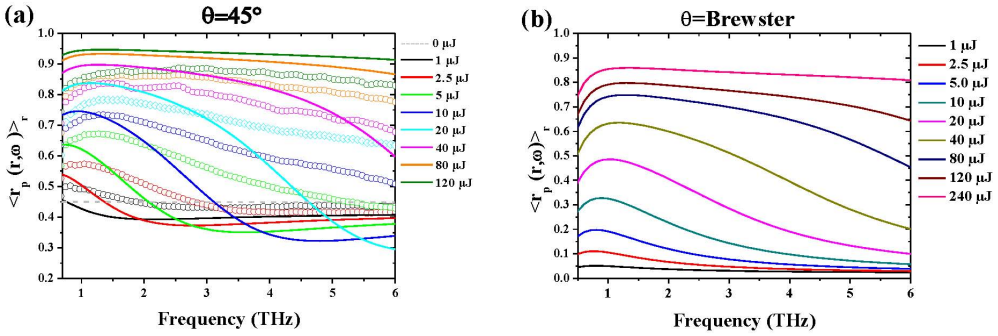

Fig. 7. a) Computed (lines) and experimental (dots) evolution of the reflection coefficient of photoexcited air/HRSi interface at 45° angle of incidence for a p-polarized THz wave versus the pump pulse energy. The p-polarized pump pulse is collinear with the THz wave. b) Computed evolution of the reflection coefficient of photoexcited air/HRSi interface at Brewster's angle of incidence for a p-polarized THz wave versus the pump pulse energy. The p-polarized pump pulse is collinear with the THz wave. When unexcited the reflection coefficient of air/HRSi interface is null.

the THz wave. The computations were performed integrating over the spatial profile of the pump and THz pulses. Experimental and numerical data display the same trends. For low pump pulse energies and above a cutting frequency, the reflection coefficient of air/HRSi interface decreases below its unexcited value ($r_p \sim 0.45$). Experimental and numerical reflection coefficients agree well above the cutting frequency. The reflection rapidly increases with E_p and it is above 0.8 in a broad spectral range when $E_p > 80\,\mu\text{J}$. For high pump pulse energies, the experimental and computed reflection coefficients deviate from each other. As we previously mentioned, this behavior is likely due to the deviation from a Gaussian spatial distribution of the actual THz beam generated in emission from two-color laser-induced air plasma filaments. At Brewster's angle, the reflection coefficient rapidly increases with the pump pulse energy and it is larger than 10% when $E_p = 2.5\,\mu\text{J}$. When $E_p > 40\,\mu\text{J}$, the reflection coefficient is higher than 70% and almost flat on a broad spectral range. The reflection coefficient can even be made as large as 85% for pump pulse energy of $120\,\mu\text{J}$ whose average fluence is $\sim 8 \times 10^{-3}\,\text{J} \cdot \text{cm}^{-2}$ quite below the damage threshold $\sim 0.2\,\text{J} \cdot \text{cm}^{-2}$ of HRSi [21]. This latter remark is important since a HRSi wafer is often placed at Brewster's angle to filter out the THz pulse generated by two-color femtosecond filament for the remaining IR pump pulse (see Fig. 1).

5. Conclusion

We have measured the evolution of the transmission and reflection coefficients of an ultrashort THz pulse incident on a HRSi wafer upon excitation by amplified Ti:Sapphire femtosecond laser pulse. The latter creates carriers that modify the dielectric constant of the HRSi wafer. For pump laser fluence quite below the damage threshold of HRSi and in the THz frequency range, large variations of the reflection and transmission coefficients of this material are recorded. The latter happens in ~ 1 ps and remains ~ 1 ns. When the carrier density is at steady state, we provide an analytical expression for the latter coefficients which can be easily extended to other kinds of semiconducting materials. This makes it possible to design on ultrafast, broadband and tunable density filters or reflectors in the THz frequency range. We have also shown that special attention has to be paid regarding the beam size of the pump and THz pulses. When both are close in size, one has to provide the spatial profile of both the pump and THz pulses incident on the HRSi wafer to properly account for the change in reflection and transmission coefficients. It is worth mentioning this phenomenon opens a new route to structure or filter on demand the spatial and spectral profile of a THz pulse.

Funding. Bordeaux International Support.

Disclosures. The authors declare no conflicts of interest.

Data availability. Data underlying the results presented in this paper are not publicly available at this time but may be obtained from the authors upon reasonable request.

References

1. J. Dai, J. Zhang, W. Zhang, and D. Grischkowsky, "Terahertz time-domain spectroscopy characterization of the far-infrared absorption and index of refraction of high-resistivity, float-zone silicon," J. Opt. Soc. Am. B **21**, 1379–1386 (2004).
2. M. van Exter and D. Grischkowsky, "Carrier dynamics of electrons and holes in moderately doped silicon," Phys. Rev. B **41**, 12140–12149 (1990).
3. J. Zielbauer and M. Wegener, "Ultrafast optical pump THz-probe spectroscopy on silicon," Appl. Phys. Lett. **68**, 1223–1225 (1996). Publisher: American Institute of Physics.
4. L. Fekete, J. Y. Hlinka, F. Kadlec, P. Kužel, and P. Mounaix, "Active optical control of the terahertz reflectivity of high-resistivity semiconductors," Opt. Lett. **30**, 1992–1994 (2005).
5. M. F. Doty, B. E. Cole, B. T. King, and M. S. Sherwin, "Wavelength-specific laser-activated switches for improved contrast ratio in generation of short THz pulses," Rev. Sci. Instruments **75**, 2921–2925 (2004).
6. J. F. Picard, S. C. Schaub, G. Rosenzweig, J. C. Stephens, M. A. Shapiro, and R. J. Temkin, "Laser-driven semiconductor switch for generating nanosecond pulses from a megawatt gyrotron," Appl. Phys. Lett. **114**, 164102 (2019).

7. G. Li, D. Li, Z. Jin, and G. Ma, "Photocarriers dynamics in silicon wafer studied with optical-pump terahertz-probe spectroscopy," Opt. Commun. **285**, 4102–4106 (2012).
8. H. Bergner, V. Brückner, and B. Schröder, "Spatially inhomogeneous carrier concentration dependence of the reflectivity of semiconductors," Opt. Quantum Electron. **14**, 245–251 (1982).
9. S. Kumar, A. Singh, S. Kumar, A. Nivedan, M. Tondusson, J. Degert, J. Oberlé, S. J. Yun, Y. H. Lee, and E. Freysz, "Enhancement in optically induced ultrafast thz response of mose2mos2 heterobilayer," Opt. Express **29**, 4181–4190 (2021).
10. S. Kumar, A. Singh, A. Nivedan, S. Kumar, S. J. Yun, Y. H. Lee, M. Tondusson, J. Degert, J. Oberle, and E. Freysz, "Sub-bandgap activated charges transfer in a graphene-MoS_2-graphene heterostructure," Nano Sel. **2**, 2019–2028 (2021).
11. L. Duvillaret, F. Garet, and J.-L. Coutaz, "A reliable method for extraction of material parameters in terahertz time-domain spectroscopy," IEEE J. Sel. Top. Quantum Electron. **2**, 739–746 (1996).
12. M. Schall and P. U. Jepsen, "Photoexcited GaAs surfaces studied by transient terahertz time-domain spectroscopy," Opt. Lett. **25**, 13–15 (2000).
13. M. Born and E. Wolf, *Principles of optics: electromagnetic theory of propagation, interference and diffraction of light* (Cambridge University Press, 1999), 7th ed.
14. Y. S. You, T. I. Oh, and K. Y. Kim, "Off-Axis Phase-Matched Terahertz Emission from Two-Color Laser-Induced Plasma Filaments," Phys. Rev. Lett. **109**, 183902 (2012).
15. E. Wang, Y. Wang, W. Sun, X. Wang, S. Feng, P. Han, J. Ye, and Y. Zhang, "Spatiotemporal Distribution Characterization for Terahertz Waves Generated From Plasma Induced by Two-Color Pulses," Front. Phys. **9**, 768186 (2021).
16. C. B. Sørensen, L. Guiramand, J. Degert, M. Tondusson, E. Skovsen, E. Freysz, and E. Abraham, "Conical versus gaussian terahertz emission from two-color laser-induced air plasma filaments," Opt. Lett. **45**, 2132–2135 (2020).
17. V. Blank, M. D. Thomson, and H. G. Roskos, "Spatio-spectral characteristics of ultra-broadband THz emission from two-colour photoexcited gas plasmas and their impact for nonlinear spectroscopy," New J. Phys. **15**, 075023 (2013).
18. A. Gorodetsky, A. D. Koulouklidis, M. Massaouti, and S. Tzortzakis, "Physics of the conical broadband terahertz emission from two-color laser-induced plasma filaments," Phys. Rev. A **89**, 033838 (2014).
19. D. E. Shipilo, N. A. Panov, I. A. Nikolaeva, A. A. Ushakov, P. A. Chizhov, K. A. Mamaeva, V. V. Bukin, S. V. Garnov, and O. G. Kosareva, "Low-Frequency Content of THz Emission from Two-Color Femtosecond Filament," Photonics **9**, 17 (2021).
20. P. Klarskov, A. C. Strikwerda, K. Iwaszczuk, and P. U. Jepsen, "Experimental three-dimensional beam profiling and modeling of a terahertz beam generated from a two-color air plasma," New J. Phys. **15**, 075012 (2013).
21. D. Tran, H. Zheng, Y. Lam, V. Murukeshan, J. Chai, and D. Hardt, "Femtosecond laser-induced damage morphologies of crystalline silicon by sub-threshold pulses," Opt. Lasers Eng. **43**, 977–986 (2005).